J|A|C|S
ARTICLES
Published on Web 12/16/2005

Anion-Promoted Cation Motion and Conduction in Zeolites

Edgar Jordan,[†] Robert G. Bell,[‡] Dirk Wilmer,[†] and Hubert Koller*,[†]

Contribution from the Institute of Physical Chemistry and Sonderforschungsbereich 458, University of Münster, Corrensstr. 36, 48149 Münster, Germany, and Davy Faraday Research Laboratory, The Royal Institution, 21 Albemarle Street, London W1S 4BS, United Kingdom

Received July 31, 2005; E-mail: hubert.koller@uni-muenster.de

Abstract: The motion of sodium cations in sodalite and cancrinite has been investigated by force field calculations, solid-state NMR, and impedance spectroscopy. Special emphasis is dedicated to the influence of anions on sodium mobilities. Local cation motion is promoted when they interact with anions. However, not all systems with high local mobilities exhibit good ion conductivities, as cooperativity of the motion appears to be an important factor, as well. The activation barrier for local sodium motion (calculations) and long-range transport (dc conductivities) is lowered in sodalite when halogenide anions, Cl^-, Br^-, or I^-, are present. The activation barriers increase with increasing size of the anion and decreasing coordination in the transition state. On the basis of ^{23}Na solid-state NMR data, all the sodium ions in the dense sodalite structure are rather rigid up to 470 K. All the cations in chromate sodalite, and Na^+ in the small cancrinite ϵ-cages without anion interactions, show a restricted local motion at higher temperatures. There is a selective high local motion of Na^+ in the neighborhood of chromate anions in the more open channel system of cancrinite. These results suggest that sodium migration can be enhanced, at least locally, in open channel systems by anion interactions. A dynamics coupling between anion reorientation and cation mobility was not observed.

Introduction

Zeolites are porous aluminosilicates with charge-balancing cations in their extraframework voids.[1−3] The number density of these extraframework cations depends on the charge density of the aluminosilicate framework (number of Al atoms in tetrahedral position per unit cell), and their nature can be varied by ion exchange. According to the Loewenstein rule,[4] a maximum of 50% of the tetrahedral centers in the framework can be occupied by Al. Typically, alkali ions are used as the charge-balancing cations in the synthesis of zeolites with high charge densities. By postsynthetic NH_4^+ exchange and subsequent calcination, protons can be exchanged for the alkali ions to generate Brønsted sites which are important in catalytic processes as solid acids. The location of the extraframework cations has been well investigated by several methods, such as X-ray and neutron diffraction methods[5] and solid-state NMR.[6,7] The majority of alkali cations are located near the center of six-ring windows of the zeolite framework (six-ring means six Si or Al atoms connected by six oxygens to form a ring). Other typical but less abundant cation sites are near four-rings, especially in alkali-rich zeolites, and other sites near larger ring-openings or in cavities of the framework. Five-rings are rare in high-alumina zeolites.

The ionic conductivity of several common zeolite framework types with alkali ions has been investigated in the past. There are only few reports,[8−17] although the high number of extraframework cations for high-alumina zeolites would imply that they are good ion conductors. Despite the presence of extraframework alkali cations, the conductivity of these materials was surprisingly poor. To date, there is no clear rationale behind this observation, and a systematic investigation of the limiting factors of ionic motion and conduction in zeolites would open new possibilities to design new ion conducting porous materials. Ion conducting zeolites would combine defined porosity with high ionic mobility. This would make them interesting candidates for applications, such as gas sensor materials or ion selective electrodes.

[†] University of Münster.
[‡] Davy Faraday Research Laboratory.

(1) Barrer, R. M. *Hydrothermal Chemistry of Zeolites*; Academic Press: London, 1982.
(2) Van Bekkum, H.; Flanigen, E. M.; Jansen, J. C. *Introduction to Zeolite Science and Practice*; Elsevier: Amsterdam, 1991.
(3) Dyer, A. *An Introduction to Zeolite Molecular Sieves*; John Wiley & Sons: Chichester, U.K., 1988.
(4) Loewenstein, W. *Am. Mineral.* **1954**, *39*, 92.
(5) Mortier, W. J. *Compilation of Extra Framework Sites in Zeolites*; Butterworth: Guildford, U.K., 1982.
(6) Hunger, M.; Engelhardt, G.; Koller, H.; Weitkamp J. *Solid State NMR* **1993**, *2*, 111.
(7) Engelhardt, G.; Hunger, M.; Koller, H.; Weitkamp, J. *Stud. Surf. Sci. Catal.* **1994**, *84*, 421.
(8) Kelemen, G.; Lortz, W.; Schön, G. *J. Mater. Sci.* **1989**, *24*, 333.
(9) Kelemen, G.; Schön, G. *J. Mater. Sci.* **1992**, *27*, 6036.
(10) Rolison, D. R. *Chem. Rev.* **1990**, *90*, 867.
(11) Freeman, D. C.; Stamires, D. N., Jr. *J. Chem. Phys.* **1961**, *35*, 799.
(12) Nischwitz, P.; Amels, P.; Fetting, F. *Solid State Ionics* **1994**, *73*, 105.
(13) Cvjeticanin, N.; Mentus, S.; Petranovic, N. *Solid State Ionics* **1991**, *47*, 111.
(14) Yamamoto, N.; Okubo, T. *Microporous Mesoporous Mater.* **2000**, *40*, 283.
(15) Barrer, R. M.; White, E. A. D. *J. Chem. Soc.* **1951**, 1267.
(16) Park, S. H.; Parise, J. B.; Gies, H.; Liu, H. M.; Grey, C. P.; Toby, B. H. *J. Am. Chem. Soc.* **2000**, *122*, 11023.
(17) Haidar, A. R.; Jonscher, A. K. *J. Chem. Soc., Faraday Trans. 1* **1986**, *82*, 3535.

10.1021/ja0551887 CCC: $33.50

Simon et al. have previously investigated the conductivity of H zeolites experimentally as well as theoretically.[18,19] With the aim to develop sensor materials, conductivities have been studied on zeolites loaded with H_2O or NH_3. The often discussed question in the zeolite community, whether trace amounts of water can drastically enhance ionic mobility, has also been investigated. The study shows that even a loading of 1 H_2O per H^+ does not increase the dc conductivity significantly. Only higher loadings show a considerable enhancement of the conductivity, which was explained by the Grotthus mechanism. NMR investigations of local proton mobility have been reviewed by Koller et al.[20] In contrast to the long-range transport as measured by dc conductivities by Simon et al., the local mobility of protons, based on NMR data, is immediately affected by small H_2O loadings.

Theoretical investigations of cation motion under the influence of $CHCl_3$ loading have been recently presented by R. G. Bell.[21] The study clearly shows that cations migrate upon chloroform loading, which is rather hydrophobic compared to water. Therefore, at least local motion is easily induced by such interactions. The groups of Grey and Auerbach have studied the cation migration in faujasite-type zeolites under the influence of hydrofluorocarbons by solid-state NMR and force field calculations.[22] Considerable migration of sodium cations from sodalite to supercages was observed and interpreted as being due to the favorable Na−F interactions.

The working hypothesis of this project is that the electrostatic interaction between sodium cations and the zeolite framework is particularly strong, if the cations are located close to the center of six-ring windows of the zeolite framework. The hopping barrier for a jump to another six-ring window is assumed to be high because the cations are localized in a deep electrostatic potential. Six-rings are preferred sites for alkali cations, in general, and this might be one reason for moderate ionic conductivities. Solid-state NMR investigations by Hunger and co-workers showed that the motion of cations in six-ring windows of zeolites X and Y begins at rather high temperatures of 570 K.[23] Further experimental support for our hypothesis can be drawn from a study by Lobo and co-workers.[24] ^{7}Li solid-state NMR and neutron diffraction experiments clearly suggest that lithium ions near the four-rings of zeolite LiX exhibit a much better local mobility than those which are located over the six-rings.

The rational search for better ion conducting zeolites requires that the fundamental elementary steps and mechanisms of ionic motion are known. To this end, two questions are raised here: (1) What are the preferred translational pathways and diffusional barriers of extraframework cations? (2) How strong is the interaction between the extraframework cations and the zeolite framework, and can it be reduced by interactions with molecules or anions? The focus of this project is to explore the elementary steps of cation motion. An important step of cation conduction is penetration through rings, which is only possible with six-rings or larger openings in the zeolite. This is an important process because it involves cations in the long-range charge transport, which are otherwise trapped in closed cages. Second, the elementary cation jump from one six-ring to another one is a prerequisite for long-range transport.

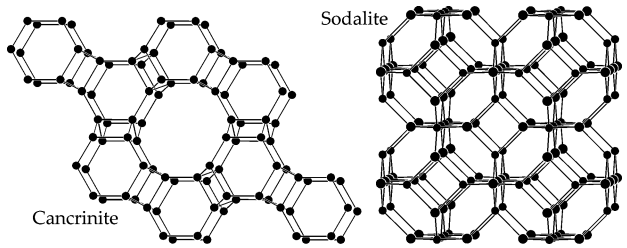

Figure 1. Comparison between the framework topologies of cancrinite and sodalite.

A promising possibility to support cation jumps is to let them interact with additional molecules or ions. This was the reason to choose sodalites with salt inclusions as ideal model systems to study the hopping mechanisms of alkali cations between six-rings when an anion is located near the hopping pathway. The sodalite structure is well suited for theoretical investigations due to its relatively simple framework structure. In this work, chromate sodalite, $|Na_4CrO_4||Na_4|[Al_3Si_3O_{12}]_2$−**SOD**, has been chosen for the experimental investigations because it has two different cage fillings, Na_4CrO_4 and Na_4. The chemical formula complies with IUPAC recommendations for zeolite nomenclature[25] with the specification that two different cage fillings are shown between vertical bars. The framework composition is in square brackets, followed by the framework type code.[26] The ^{23}Na NMR lines at room temperature are different for sodium cations located in each of the two cages.[27] An exchange between the two cages would be characterized by an exchange signal in ^{23}Na NMR spectra at elevated temperatures.

In addition, a more open structure than sodalite has been selected, which provides vacant space for cationic jump processes. Chromate cancrinite, $|Na_6CrO_4||Na_2|[Al_6Si_6O_{24}]$−**CAN**, is the ideal choice because it has the same stoichiometric composition as chromate sodalite, but with a more open framework structure. The two framework structures are shown in Figure 1. Sodalite is a dense structure without large pores because it consists of a space-filling packing of sodalite cages (capped octahedral cages). The cancrinite structure exhibits one-dimensional twelve-ring channels and small cancrinite cages (ϵ-cages), both of which contain sodium cations. The chromate anions are only located in the large channels. The sodium cations are located over six-rings in all sites. The location of the chromate anions in sodalite and cancrinite makes them two ideal model systems to investigate the sodium mobility with and without the influence of chromate anions. Although the chemical compositions of chromate sodalite and cancrinite are exactly the same, their framework topology and, consequently, the topological environments of the mobile cations differ considerably. In sodalite, the topological surroundings of the sodium cations are the same at all locations, and their coordination alters

(18) Franke, M. E.; Sierka, M.; Simon, U.; Sauer, J. *Phys. Chem. Chem. Phys.* **2002**, *4*, 5207.
(19) Franke, M. E.; Simon, U.; Moos, R.; Knezevic, A.; Müller, R.; Plog, C. *Phys. Chem. Chem. Phys.* **2003**, *5*, 5195.
(20) Koller, H.; Engelhardt, G.; Van Santen, R. A. *Top. Catal.* **1999**, *9*, 163.
(21) Ramsahye, N. A.; Bell, R. G. *J. Phys. Chem. B* **2005**, *109*, 4738.
(22) (a) Jaramillo, E.; Grey, C. P.; Auerbach, S. M. *J. Phys. Chem. B* **2001**, *105*, 12319. (b) Lim, K. H.; Grey, C. P. *J. Am. Chem. Soc.* **2000**, *122*, 9768.
(23) Hunger, M.; Schenk, U.; Buchholz, A. *J. Phys. Chem. B* **2000**, *104*, 12230.
(24) Feuerstein, M.; Lobo, R. F. *Chem. Mater.* **1998**, *10*, 2197.
(25) McCusker, L. B.; Liebau, F.; Engelhardt, G. *Pure Appl. Chem.* **2001**, *73*, 381.
(26) (a) Meier, W. M.; Olson, D. H.; Baerlocher, Chr. *Atlas of Zeolite Framework Types*, 5th ed.; Elsevier: Amsterdam, 2001. (b) http://www.iza-structure.org/databases.
(27) Engelhardt, G.; Sieger, P.; Felsche, J. *Anal. Chim. Acta* **1993**, *283*, 967.

depending on the presence of chromate anions. Therefore, sodalite is a model for a topologically homogeneous zeolite matrix with equivalent cages. In contrast, cancrinite represents the more complicated structure with two topologically different voids: one-dimensional twelve-ring channels and ϵ-cages. The influence of topological properties (framework density, free volume) on the ionic mobility can be investigated by the choice of these zeolites with the same composition.

This paper is organized in the following way. First, theoretical force field calculations on simple halogenide sodalite model systems are carried out to estimate the energetic barriers for cation migration. These theoretical investigations were included to understand the influence of anions on cation motion on a simpler system with isotropic anions. This part is then supplemented by experimental ionic conductivity studies to verify the observed theoretical trends. The second part presents the characterization of cation and anion motion in chromate sodalite by ^{23}Na solid-state NMR. The final part is dedicated to sodium mobility in chromate cancrinite, which is a more open framework structure, and Na^+ mobility with and without the influence of an anion is addressed. It will be shown that cation−anion interaction is a potential promoter for local mobilities, which is most pronounced in the open channel system of cancrinite.

Experimental Section

Synthesis. Chloride sodalite was synthesized under hydrothermal conditions from kaolinite and sodium chloride in basic solution. Five grams of kaolinite and 5.85 g of sodium chloride were mixed and transferred into 50 mL Teflon-lined steel autoclaves. The autoclaves were filled to 95% with an 8 M solution of carbonate-free sodium hydroxide. Similar procedures have been employed for the other halogenides, Br^- and I^-. All reactions were carried out under autogenous pressure at 200 °C for 7 days. During the synthesis, the autoclaves were slowly rotated (30 rpm) to ensure uniform mixing. The obtained halogenide sodalites were washed with water until its pH value was neutral.

Chromate cancrinite was synthesized under hydrothermal conditions by carefully mixing 1.87 g of SiO_2 and 1.59 g of Al_2O_3 with an excess of 14.04 g of sodium chromate. The mixture was then transferred into 50 mL Teflon-lined steel autoclaves. The autoclaves were filled to 95% with an 8 M solution of carbonate-free sodium hydroxide. The reaction was carried out under autogenous pressure at 200 °C for 7 days under slow rotation (30 rpm).

Chromate sodalite was synthesized from chromate cancrinite by a solid-state phase transformation with an excess of Na_2CrO_4. Cancrinite was mixed with anhydrous sodium chromate (1:1 w/w) and slowly heated to 970 °C for 72 h. The addition of Na_2CrO_4 was needed to avoid chromate occupancies to decrease in the solid-state transformation. The resulting product was ground and washed with distilled water to remove sodium chromate. The yellow, insoluble residue was dried overnight at 80 °C. Crystallinity and phase purity of all reaction products were verified by powder X-ray diffraction and ^{29}Si MAS NMR.

The ^{17}O-enriched sample of chromate cancrinite was prepared by using 40% ^{17}O-enriched water for the hydrothermal synthesis. As the oxygen would exchange with the air during thermal treatment, ^{17}O enrichment of the chromate sodalite was achieved by hydrothermal treatment of the as-made chromate sodalite with 40% ^{17}O-enriched water at 100 °C for 24 h. The crystallinity of the sodalite was not affected by this procedure according to X-ray diffraction.

Prior to NMR and conductivity measurements, all samples had to be carefully dehydrated. Dehydration was achieved by heating the samples under vacuum at 300 °C for 12 h in glass ampules. The absence of water was verified by ^{1}H MAS NMR.

Solid-State NMR. The ^{29}Si MAS NMR spectra were recorded on a Bruker CXP NMR spectrometer at a field of 7.05 T with a ^{29}Si resonance frequency of 59.6 MHz and MAS speed of 4 kHz. ^{23}Na MAS NMR spectra were recorded on Bruker DSX NMR spectrometers at magnetic fields of 9.4 or 11.7 T with ^{23}Na resonance frequencies of 105.8 or 132.3 MHz. The spinning speeds were selected between 8 and 12 kHz. Static ^{23}Na NMR spectra were acquired at 4.7, 7.05, and 9.4 T. Chemical shifts were referenced to TMS (^{29}Si), 1 M NaCl (^{23}Na), and H_2O (^{17}O). For the quadrupolar nuclei, ^{17}O and ^{23}Na, a radio frequency field of 62 kHz and pulse lengths of 0.6 μs were employed to ensure quantitative excitation conditions.

Conductivity Measurements. Conductivity measurements were performed using a Novocontrol Alpha high-resolution dielectric analyzer between room temperature and 573 K in a frequency range from 10^{-2} Hz to 3 MHz. For the impedance measurements, the as-made samples were ball-milled, dehydrated as described above, transferred into an airtight pressing tool under argon atmosphere, and pressed to tablets. The resulting samples were sputtered with gold and then transferred into the measurement cell.

Force Field Calculations. The force field calculations were carried out using the General Utility Lattice Program (Gulp).[28] In a first step, the ordered sodalite structures were allowed to relax to equilibrium without any symmetry constraints. Thereafter, sodium vacancies were created by the removal of a single sodium atom from the structure. The surrounding lattice was allowed to relax again under the influence of the defect. The energy differences between the relaxed structures without and with a sodium point defect were taken as defect energies for a sodium site.

The trajectories on which neighboring sodium atoms moved toward the point defect were simulated by moving the sodium atom stepwise along one Cartesian direction from its initial position toward the vacancy, while allowing relaxation of the surrounding structure as well as relaxation of the sodium position in the two other Cartesian directions. The defect energy minimization of such diffusional steps led to the energy barriers for the cation movement.

Results and Discussion

Force Field Calculations and Conductivity Measurements of Halogenide Sodalites. The anion influence on local cation motion is first studied by simple theoretical investigations. By means of force field calculations, we were able to compare diffusion barriers of the "empty" sodalite, $|Na_6|[Al_6Si_6O_{24}]$, and the halogenide sodalites, $|Na_8Hal_2|[Al_6Si_6O_{24}]$, Hal being either chloride, bromide, or iodide. The sodalite cage consists of eight six-ring windows and six four-ring units (Figure 1). The sodium cations are located on 3-fold axes above the six-ring centers, and the halogenide anions are in the center of the sodalite cage. Only four sodium cations can be accommodated in one cage, and the cations in the neighboring cages have to localize at the alternate four six-rings. As the sodium sublattice of the halogenide sodalites is fully occupied, cation defects have to be introduced prior to the simulation of any motional process. The creation of a sodium point defect is a quite energy-consuming process; the defect energies range from 639 kJ mol^{-1} for the iodide sodalite to 661 kJ mol^{-1} for the chloride sodalite. The formation of a vacancy was not needed for the anion-free sodalite, which is intrinsically disordered, as each sodalite cage contains only three instead of four possible sodium cations.

In the case of the halogenide sodalites, two different motional processes were studied (Figures 2 and 3). In the first scenario, a sodium cation moved from its crystallographic site toward a defect site in the same sodalite cage by passing the anion in

(28) Gale, J. D. *J. Chem. Soc., Faraday Trans.* **1997**, *93*, 629.

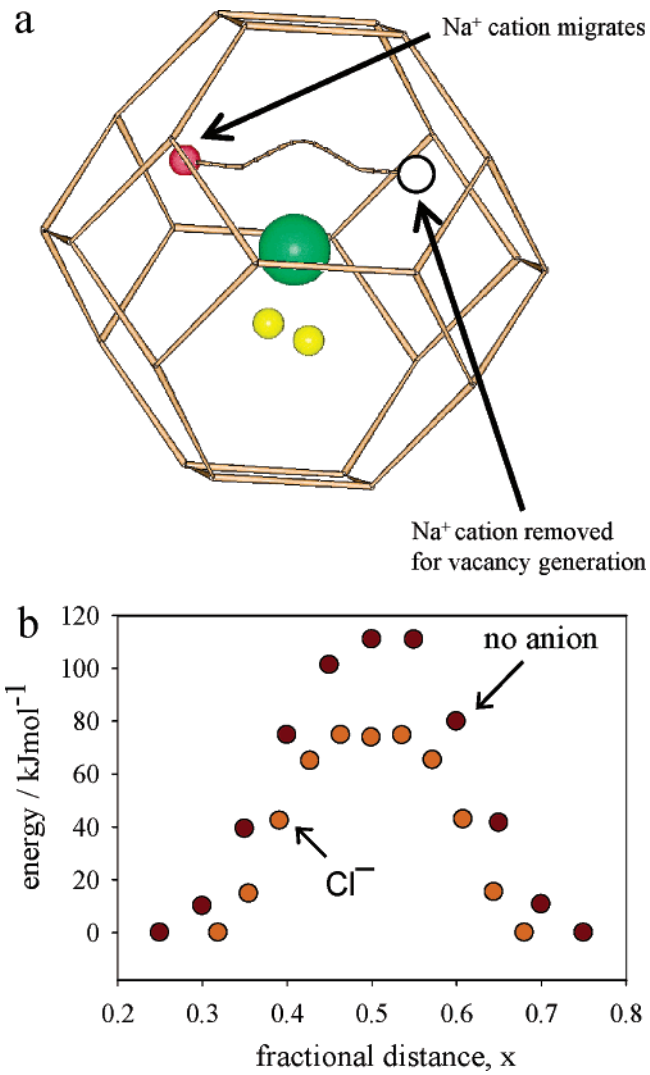

Figure 2. (a) Calculated diffusional pathway in halogenide sodalite for intracage motion of sodium cations; (b) energy for this movement with Cl^- in the cage center or without anion.

the center of the cage (Figure 2a). The diffusional path for this motion is along the four-ring between the two six-rings. In the second scenario (Figure 3a), the vacancy was refilled by a sodium cation from a neighboring cage by first penetrating the aluminosilicate six-ring window and subsequent passage of the halogenide. The latter is necessary due to alternating occupancy of the eight six-rings in both cages. The intracage anion passage of this diffusional path does not lead over a four-ring, as it passes the edge between two six-rings.

Figure 2b illustrates two main influences of the chloride anion. The energetic barrier for the motional trajectory shown in Figure 2a is lower than that in the anion-free cage. Second, the diffusional distance is smaller in the cage with chloride, as the sodium cations are localized less deep in the six-ring windows. Interestingly, ring penetration needs less activation than the intracage movement between six-rings (Figure 3b). Chloride sodalite showed the lowest energy barriers for both types of cation motion, 75.1 kJ mol^{-1} for the intracage motion and 97.4 kJ mol^{-1} for the penetration of the six-ring and subsequent anion passage. In both cases, the maximum of the barrier was marked by the passage of the chloride anion. Therefore, it is not surprising that the energy barriers rise with increasing ionic

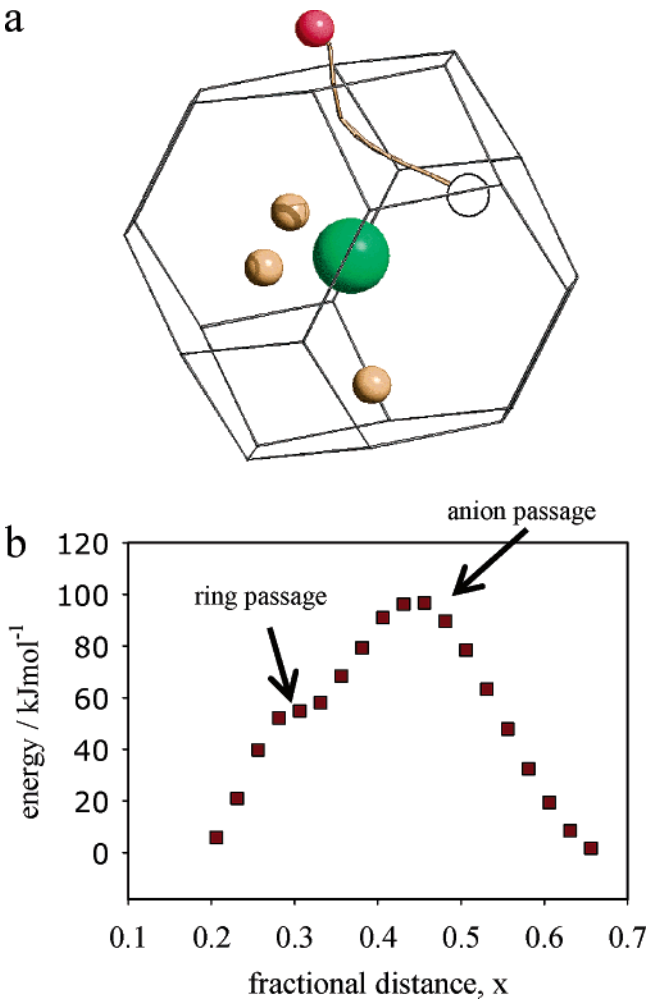

Figure 3. (a) Calculated diffusional pathway in chloride sodalite for intercage motion of sodium cations; (b) energy landscape for this movement.

Table 1. Total Defect Energies (in kJ/mol) and Motional Barriers for Halogenide Sodalites and Anion-Free Sodalite (for the latter, no defects had to be created due to stoichiometrical vacancies)

	defect energy	intracage	intercage
$\|Na_4Cl\|_2\,[Al_6Si_6O_{24}]$−**SOD**	660.9	75.1	97.4
$\|Na_4Br\|_2[Al_6Si_6O_{24}]$−**SOD**	652.4	101.3	105.2
$\|Na_4I\|_2[Al_6Si_6O_{24}]$−**SOD**	638.5	101.3	114.8
$\|Na_3\|_2[Al_6Si_6O_{24}]$−**SOD**	n.d.	111.0/145.7	n.d.

radius of the halogenide (Table 1). In the trajectories calculated for both, the intracage process and the penetration of the six-ring, the steric influence of the halogenide anion can be clearly observed (Figures 2 and 3).

The movement of a neighboring sodium ion to the cation vacancy of the anion-free sodalite has an activation barrier for a trajectory via a four-ring of 111.0 kJ mol^{-1}. A simulation of a movement through the six-ring did not give a stable trajectory, as other cations began to move, as well. The intracage migration path over an edge between six-rings results in a significantly higher activation barrier of 145.7 kJ/mol. These values are significantly higher than that for the intracage motion of all halogenide sodalites and also for the passage of the six-ring in the case of chloride and bromide sodalite. The results show that the additional Coulomb interaction between the halogenide anions and the sodium cations lowers the barrier for motion between the six-rings. A comparison between the two different

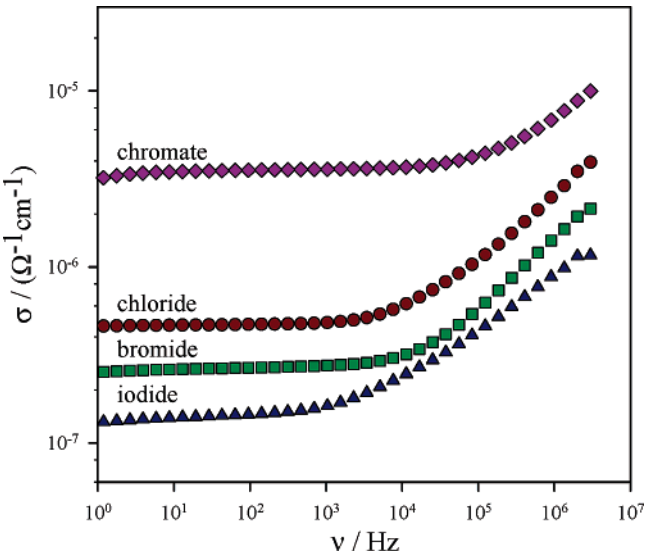

Figure 4. Frequency dependent conductivities of sodalites at 573 K, $|Na_4Cl|_2$ $[Al_6Si_6O_{24}]$−**SOD**, $|Na_4Br|_2[Al_6Si_6O_{24}]$−**SOD**, $|Na_4I|_2[Al_6Si_6O_{24}]$−**SOD**, and $|Na_4||Na_4CrO_4|$ $[Al_6Si_6O_{24}]$−**SOD**.

trajectories for the same anion shows that the anion passage is characterized by a lower activation barrier when the sodium cation migrates over a four-ring. This may be due to the more favorable coordination with oxygen in the four-ring compared to the low coordination with one oxygen only on the edge between two six-rings.

NMR investigations on halide sodalites were not conducted because chloride and bromide sodalites only show one Gaussian ^{23}Na NMR line, making investigations of intra- and intercage exchange processes difficult. Iodide sodalite has been investigated by Fechtelkord, and ^{23}Na NMR results provide evidence for cation mobility beginning at 673 K.[29] However, it is not clear whether this means intra- or intercage motion because all cations yield one NMR component only.

The conductivity measurement of the chloride sodalite resulted in an activation energy for the dc conductivity of 82.0 ± 0.8 kJ/mol, which is between the activation barriers for the two calculated elementary jump processes between the cation sites. As expected from the GULP simulations, this activation energy for dc conductivity increases with increasing anion size: 84.9 ± 1.1 kJ/mol for bromide sodalite and 88.5 ± 1.2 kJ/mol for iodide sodalite. The frequency dependent conductivities (Figure 4) show the expected trend for the dc plateau with the highest conductivity for chloride sodalite at 300 K.

At this point, the length scales of the computational study and impedance spectroscopy should be compared. Also, both methods yield the same trend, but it should be kept in mind that a vacancy was created in the calculation. The vacancy concentration in the real samples is unknown. High dc conductivities require efficient long-range transport processes. The fact that both methods show the same trend and similar activation barriers does not provide final proof that local mobilities are the only factor to be considered in ion conduction. The work shown below was carried out to further address this point.

Figure 4 also shows the frequency dependent conductivity of chromate sodalite, $|Na_4||Na_4CrO_4|$ $[Al_6Si_6O_{24}]$−**SOD**. Although the size of this anion is larger than the halides, the dc plateau shows a considerably higher conductivity. Two reasons are possible for this improvement of long-range charge transport. The complex CrO_4^{2-} anion may promote local cation jumps by its reorientational motion in the sense of a paddle-wheel mechanism,[30] or the different cage fillings offer a better scenario for long-range transport by cooperative motion of the cations. Therefore, chromate anions are now in the focus of the investigations. Unfortunately, theoretical calculations with these anions were not possible due to the lack of appropriate force field parameters. Hence, solid-state NMR will be the major tool for the study of local motion.

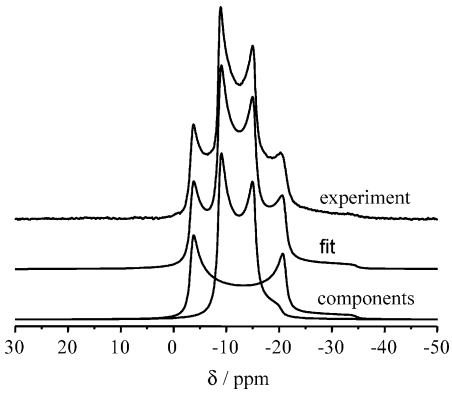

Figure 5. ^{23}Na MAS NMR spectrum at $B_0 = 9.4$ T of $|Na_4CrO_4||Na_4|[Al_6Si_6O_{24}]$−**SOD** and its simulated components. Broad component: $C_q = 2.56$ MHz, $\eta = 0$, $\delta_{cs} = 1.7$ ppm. Narrow component: $C_q = 1.56$ MHz, $\eta = 0$, $\delta_{cs} = -6.8$ ppm.

Solid-State NMR. Solid-state NMR data are now presented on more complex systems with chromate anions. Single peaks in the ^{29}Si MAS NMR spectra of the chromate cancrinite (−85.7 ppm) and sodalite (−90.7 ppm) show that the aluminosilicate framework has an n_{Si}/n_{Al} ratio of 1:1. The lines are sharp (fwhh = 95 Hz), indicating an ordered structure and a small distribution of Si−O−Al angles. This observation suggests a strict alternation of empty and chromate-loaded sodalite cages and, therefore, a complete loading of the structure with sodium chromate.[27]

The ^{23}Na MAS NMR spectrum of the chromate sodalite (Figure 5) consists of two signals with a typical line shape for second-order quadrupolar interaction. This fit was confirmed by ^{23}Na MQMAS NMR (not shown). The broad signal with a quadrupolar coupling constant of 2.56 MHz ($\eta = 0$; $\delta_{cs} = 1.7$ ppm) belongs to the sodium cations in the anion-free sodalite cages, whereas the sodium cations additionally coordinated to the chromate anions give rise to the narrower line ($C_q = 1.56$ MHz; $\eta = 0$; $\delta_{cs} = -6.8$ ppm).[27] The area ratio of the two components is 1:1, as expected for a strict alternation of chromate-occupied and anion-free cages. Surprisingly, the asymmetry parameter of both signals is zero at room temperature, indicating an axial symmetry for both sodium sites. However, for the sodium cations in the chromate-filled cages, axial symmetry is not feasible due to steric reasons. The Cr−O bond axes cannot be accommodated on the 3-fold axes of the sodalite lattice because the Na−O bond distances would then be too short. Therefore, in a static situation, the CrO_4^{2-} anion would have to be located in the center of the sodalite cages with a tilt orientation which breaks the axial symmetry on the sodium cations. Therefore, the observation of axial symmetry of the electric field gradient at sodium in ^{23}Na MAS NMR

(29) Fechtelkord, M. *Solid State NMR* **2000**, *18*, 70.

(30) Lundén, A. *Solid State Ionics* **1988**, *28*−*30*, 163.

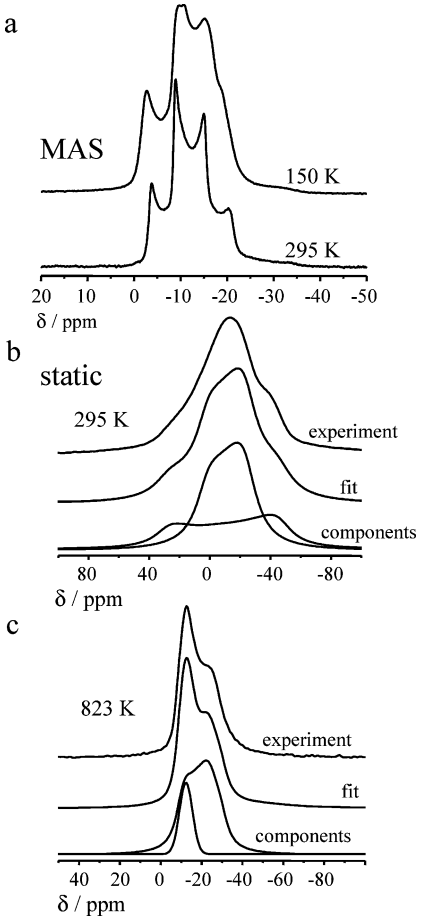

Figure 6. (a) ^{23}Na MAS NMR and static ^{23}Na NMR spectra of $|Na_4CrO_4||Na_4[Al_6Si_6O_{24}]$−**SOD** at various temperatures (B_0 = 9.4 T) with simulations at (b) 295 K, components simulated with the same parameters as in Figure 5; (c) 823 K, narrow component, Gaussian line at −12.4 ppm, fwhh = 791 Hz; broad component, $\delta_{cs} = -16.1$ ppm, $C_q = 1.22$ MHz, $\eta = 0.36$.

spectra can only be achieved by a dynamic disorder of the central anion. ^{17}O NMR experiments have been employed to prove this assumption (see below).

Figure 6 shows ^{23}Na NMR spectra of chromate sodalite at various temperatures. While the spectra at 295 and 150 K have been acquired under MAS conditions (Figure 6a), Figure 6b,c shows ^{23}Na NMR spectra without sample rotation and their simulations. These static NMR spectra have enabled us to achieve higher temperatures than with magic angle spinning. The low-temperature ^{23}Na MAS NMR spectrum at 150 K shows some broadening of the two components with a splitting of a singularity in the center. Despite our attempts to simulate this experiment, also by using different magnetic field strengths, we are not confident to suggest an unambiguous model as yet. The spectrum at 150 K is possibly affected by a splitting of the ^{23}Na NMR component of the sodium cations in the chromate-filled cage, which is indicated by the splitting of the singularity in the center. In addition, as ^{17}O NMR data reveal (see below), there are cages with mobile and rigid chromate anions at this temperature, which complicates the situation. The accumulation of a better resolved MQMAS spectrum at 150 K has not been possible due to the long measuring time. Nevertheless, the general peak shape broadening and singularity splitting clearly indicate a change at low temperature, which originates from a freezing of the anion motion (see below).

There is no clear NMR evidence for exchange dynamics between the two cages upon heating the sample up to 823 K. The static ^{23}Na NMR spectrum at this temperature can be simulated with a Gaussian component at −12.4 ppm and a quadrupolar component with $C_q = 1.22$ MHz, $\eta = 0.36$, and $\delta_{cs} = -16.1$ ppm. This simulation is confirmed at two different magnetic fields of B_0 = 9.4 and 7.05 T. An analysis of the evolution of chemical shifts for both components over the entire temperature range results in the assignment of the Gaussian component to the sodium cations in the chromate-filled cage, and the quadrupolar component is due to the sodium cations in the anion-free cage. The narrowing of both quadrupolar components indicates a dynamic averaging of their quadrupolar interactions. A complete exchange between the cages would yield an averaging of both NMR components, which is not observed. The quadrupole coupling constant for the anion-free cage is reduced from its original value (2.56 MHz) by a factor of 0.48. This dynamic averaging factor is close to the value of 0.5, which can be due to a two-site jump by an angle between 70 and 110°.[31] An intracage cationic jump between two neighboring six-rings in the anion-free cages could well explain the observed reduction in quadrupolar interaction. The Gaussian line width at 823 K can also be simulated as a quadrupolar component with $C_q = 0.78$ MHz, yielding the same line width. Therefore, the dynamic narrowing factor of about 0.5 for this component is similar to the one of the broader line. In summary, an analysis of the reduction in line width for both components over the entire temperature range shows that the extent of dynamic averaging and the onset temperature are the same for both lines. This important result on the dense chromate sodalite indicates that cation mobilities are not independent, or are even coupled to each other.

The relatively high dc conductivities of chromate sodalite (Figure 4) are not reflected by an unambiguous intercage exchange in the NMR data. This may be due to the different time scales of NMR and impedance spectroscopies. Next, the possible effect of anion reorientation on cation mobility is investigated.

To further elucidate the anion motion, ^{17}O NMR investigations have been undertaken. Figure 7 shows the static spectra at 295 and 140 K. Due to their nuclear electric quadrupole moment, a very high quadrupole interaction is expected for ^{17}O nuclei in CrO_4^{2-}. However, the ^{17}O NMR spectrum at 295 K shows a relatively sharp Gaussian line at δ = 789.4 ppm (fwhh = 1293 Hz), which can only be explained by a high mobility of the chromate anions. The line shape does not change much, that is, a minor broadening can be observed, upon lowering the temperature. However, the line intensity at 140 K is dramatically reduced. The intensities in the entire temperature range are also shown in Figure 7. They increase upon lowering the temperature from 275 to 215 K as expected from the temperature dependence of energy level occupancies,[32] but then the signal decreases upon further lowering the temperature. This can only be due to an extreme line broadening beyond the limit of detection. Effects from T_1 relaxation times have been ruled out. The ^{17}O NMR line broadens due to a large quadrupolar interaction for the chromate anions, which are frozen out. The narrow component

(31) Schmidt-Rohr, K.; Spiess, H. W. *Multidimensional Solid-State NMR and Polymers*; Academic Press: London, 1994.
(32) Abragam, A. *Principles of Nuclear Magnetism*; Clarendon Press: Oxford, 1996.

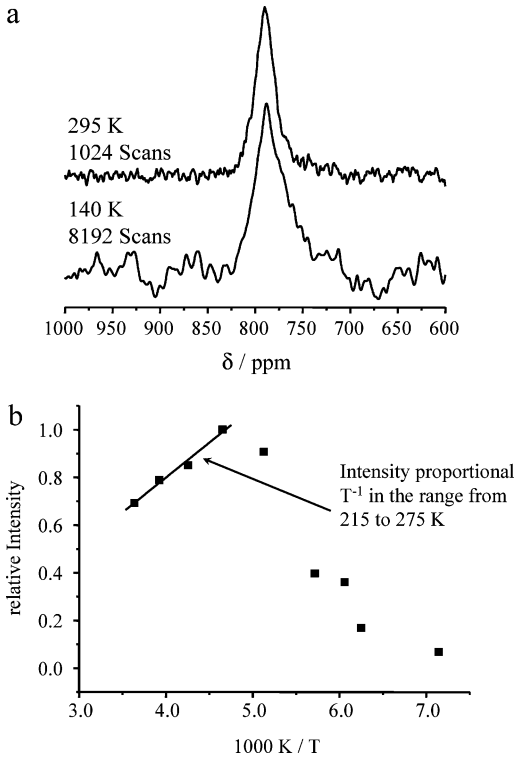

Figure 7. (a) Static ^{17}O NMR spectra ($B_0 = 9.4$ T) of chromate anions in $|Na_4CrO_4||Na_4|[Al_3Si_3O_{12}]_2$−**SOD** (peaks from framework oxygen are not shown), (b) and their temperature-dependent line intensities.

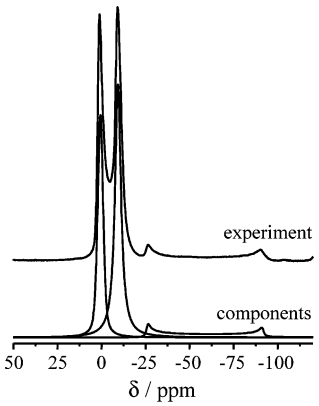

Figure 8. ^{23}Na MAS NMR spectrum ($B_0 = 9.4$ T) of $|Na_6CrO_4||Na_2|[Al_6Si_6O_{24}]$−**CAN** along with fitted components; Gaussian components at 1.4 and −9.3 ppm, and broad second-order quadrupolar line with $C_q = 4.96$ MHz, $\eta = 0$, and $\delta_{cs} = -6.7$ ppm.

which is still visible at low temperature is due to the remaining anions with high mobility. The large temperature range over which these changes occur shows that this event is not a discrete first-order phase transition. Interestingly, the drop in ^{17}O NMR signal intensity occurs at the same temperature, where the ^{23}Na MAS NMR spectra show a broadening and singularity splitting for the component which is assigned to chromate-filled cages. This suggests that the ^{23}Na MAS NMR line shapes at low temperatures are influenced by the anion motion, and not by a change in cation dynamics.

The ^{23}Na and ^{17}O NMR investigations of chromate sodalite result in the conclusion that there is no obvious correlation between cation and anion mobilities. The chromate anions are highly mobile at room temperature down to 215 K, but the sodium cations are rigid at these temperatures on the NMR time scale. This observation makes it less likely that the dc conductivities are enhanced by an anion-accelerated local mobility of the cations. On the other hand, the local cation motion increases at higher temperatures for both, the cages with and without chromate. A cooperative mechanism of cationic motion is obviously responsible for the higher conductivity. A possible explanation for the improved conductivity compared to the halide sodalites may be that there are anion-free cages in chromate sodalite which allow for a defect mechanism involving interstitial sites. The topology of sodalite and cancrinite is the next factor to be investigated.

Therefore, such investigations are now extended to chromate cancrinite, which has the same chemical compositions as chromate sodalite, but with a more open pore structure and two topologically different voids. This zeolite will also be investigated in terms of anion mobility, cooperative onset of local cation motion, and dc conductivity. Figure 8 shows the ^{23}Na MAS NMR spectrum of cancrinite at room temperature ($B_0 = 9.4$ T). Three components are observed, two very sharp peaks at 1.4 and −9.3 ppm (fwhh = 399 and 394 Hz, respectively) and a broad quadrupolar line with $C_q = 4.96$ MHz, $\eta = 0$, and $\delta_{cs} = -6.7$ ppm. ^{23}Na NMR experiments at other magnetic fields confirm the presence of these components. This clear resolution of three components is rare in ^{23}Na solid-state NMR. According to electric field gradient calculations,[33] the large quadrupole coupling constant of 4.96 MHz is typical for sodium cations in zeolite six-ring windows without extraframework anion interaction. Therefore, this broad component can be straightforwardly assigned to the sodium cations at six-ring windows in the anion-free cancrinite cages. The sharp Gaussian lines are assigned to two different sodium positions in the twelve-ring channels in which the chromate anions are located. Crystallographic structure data of chromate cancrinite are not available. Crystal structures of cancrinites with other anions, CO_3^{2-} or SO_4^{2-}, are published with only one sodium position in the large channels.[34,35] However, anion vacancies cause a cation superstructure, which is possibly not properly described by the employed space group symmetry, leading to a second sodium position. Therefore, the ^{23}Na NMR data of this work and further experiments on sulfate cancrinite (not shown) clearly yield more than two sodium positions in total, that is, two in the large channel and one in the ϵ-cage (two for sulfate cancrinite). This suggests that the structure descriptions of these cancrinites need further improvement in terms of symmetry and number of sodium sites.

The dynamic properties of the sodium cations with and without anion interaction in one single cancrinite structure are now investigated separately. Figure 9 shows the ^{23}Na MAS NMR spectra of chromate cancrinite, which focus on the two narrow lines at elevated temperatures (Figure 9a) and a two-dimensional ^{23}Na exchange MAS NMR spectrum (EXSY: $\pi/2$-t_1-$\pi/4$-τ_m-$\pi/4$-acquire) at 350 K (Figure 9b). The MAS NMR spectra from 350 to 470 K clearly show evidence for a dynamic exchange process between the two sharp lines. An additional line between these two peaks appears at 380 K, which grows upon increasing the temperature, accompanied by a reduction

(33) Koller, H.; Engelhardt, G.; Kentgens, A. P. M.; Sauer, J. *J. Phys. Chem.* **1994**, *98*, 1544.
(34) Hassan, I.; Grundy, H. D. *Can. Mineral.* **1984**, *22*, 333.
(35) Hackbarth, K.; Gesing, Th. M.; Fechtelkord, M.; Stief, F.; Buhl, J. Chr. *Microporous Mesoporous Mater.* **1999**, *30*, 347.

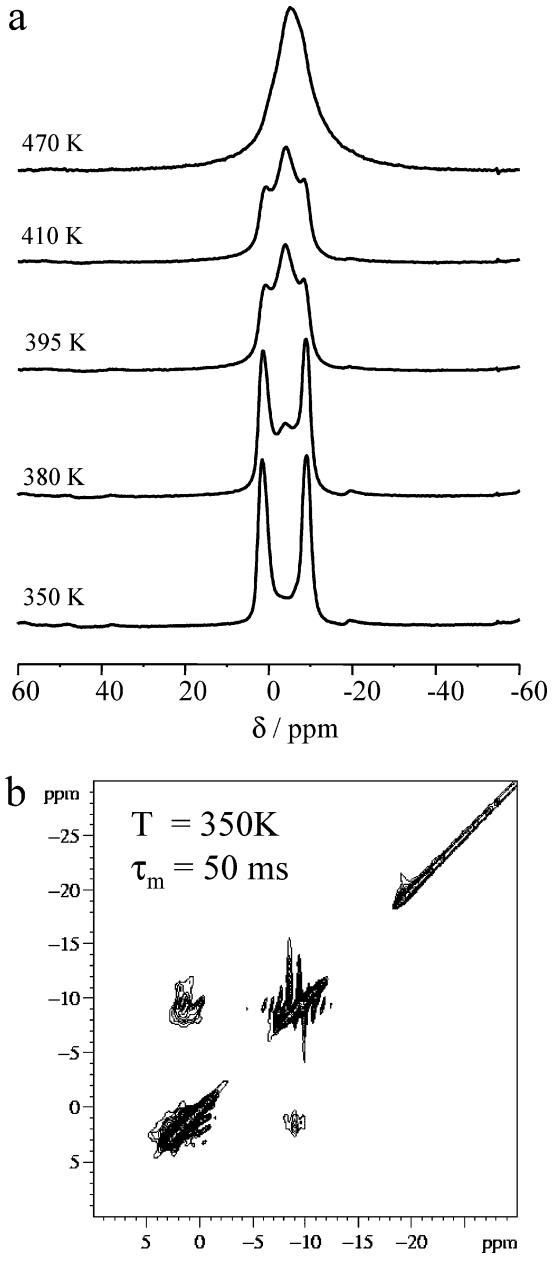

Figure 9. (a) Variable temperature ^{23}Na MAS NMR, (b) and 2D EXSY spectra of $|Na_6CrO_4||Na_2|[Al_6Si_6O_{24}]$−**CAN** ($B_0$ = 11.7 T).

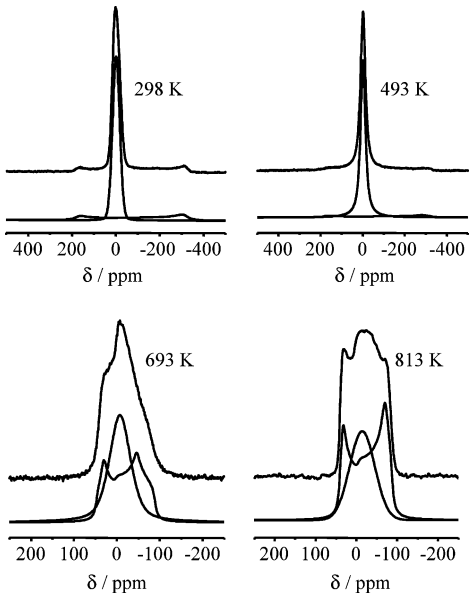

Figure 10. Static ^{23}Na VT echo NMR spectra (B_0 = 7.05 T) of $|Na_6CrO_4||Na_2|[Al_6Si_6O_{24}]$−**CAN** with simulations, 295 K: Gaussian line at δ = −5.22 ppm (fwhh = 3079 Hz), quadrupolar line with δ_{cs} = −7.0 ppm, C_q = 4.87 MHz, η = 0; 823 K: Gaussian line at δ = −17.9 ppm (fwhh = 5732 Hz), quadrupolar line with δ_{cs} = −8.6 ppm, C_q = 2.35 MHz, η = 0.1.

of the two original lines. At 470 K, only the exchange peak is visible. These spectra do not show the typical coalescence behavior in which the two originating peaks move toward each other and merge finally at the coalescence temperature. Here, the peak positions remain nearly unchanged over the entire temperature range. This observation can be explained by a dynamic heterogeneity with a distribution of correlation times. There are fast sodium cations which exchange on the NMR time scale, which is the chemical shift difference between the two starting signals (ca. 1400 Hz), yielding the exchange peak in the center. In addition, there are slow sodium cations which do not exchange on this time scale. The relative number density of cations in the fast correlation time regime increases at higher temperatures, thus increasing the intensity of the exchange signal. There is no indication that the broad quadrupolar component participates in this exchange process up to the temperature of 470 K. Although the quadrupolar line broadens at elevated temperatures, the peak position of the exchange peak between the two narrow signals does not move, which would be expected if the quadrupolar signal would participate in this particular dynamics.

The exchange process of the narrow lines is verified in the two-dimensional EXSY experiment (Figure 9b). The peaks on the diagonal of the two-dimensional spectrum correspond to the signals in the one-dimensional spectrum. Any off-diagonal peaks indicate an exchange process between the peaks on the diagonal to which they correspond. The off-diagonal intensities are a function of the mixing time, τ_m, which is typically in the range of several tens of milliseconds. This technique is suitable to investigate slow motional processes. Therefore, it has to be performed at a temperature at which the two original peaks still dominate the spectrum, but the exchange process already begins to take place.

The exchange peaks between the two narrow signals are clearly identified in the two-dimensional experiment, and the broad quadrupolar component does not participate in this process. The window for mixing times and temperatures in which the exchange can be observed in the 2D experiment was rather narrow, and there are also restrictions by T_2 relaxation. These limitations did not allow us to analyze activation parameters by varying the mixing times over a wider range.

Additional information about the dynamic scenario in the cancrinite phase can be obtained from high-temperature static ^{23}Na NMR spectra (Figure 10). Due to the existence of broad lines, echo spectroscopy was employed. Therefore, the peak areas are not quantitative. At room temperature, the static ^{23}Na NMR spectrum consists of a Gaussian line and a quadrupolar powder pattern in good agreement with the MAS NMR data. The Gaussian line corresponds to the two sharp ^{23}Na NMR peaks which cannot be resolved in the static spectra of Figure

10. The broad quadrupolar line in the static room temperature spectrum can be simulated with the same parameters as in the MAS NMR experiment (see above).

At 493 K, this broad signal begins to reduce its intensity until it reappears at 693 K with a remarkably reduced quadrupolar coupling constant (Figure 10). The disappearance of this line between these temperatures is explained by the signal loss in the static echo spectra in the intermediate motional regime, which is a well-known phenomenon of this NMR technique under the influence of dynamic processes. The quadrupolar component with reduced broadening compared to the room temperature spectrum is clearly identified by the two singularities at 31.8 and −69.9 ppm at 813 K ($B_0 = 7.05$ T). The simulation of the quadrupolar line shape leads to small asymmetry parameters for both the low-temperature and the motionally averaged high-temperature spectrum. While the C_q value for the quadrupolar interaction at 298 K is 4.96 MHz, it is reduced to about one-half of its initial value at 813 K ($C_q = 2.35$ MHz, $\eta = 0.1$, $\delta_{cs} = -8.6$ ppm). This observation can be explained by a fast two-site jump of the sodium cations, which leads to a flip of the local electric field gradient by an angle close to 90°. Especially the asymmetry parameter, η, is very sensitive to two-site jump angles in this range, and it only assumes a value of $\eta = 0$ for 90°.[31] Such an environment is offered by the ϵ-cages of the cancrinite consisting of aluminosilicate six-rings perpendicular to each other. Thus, the broad line and its exchange behavior can be assigned to the sodium cations at six-ring windows in the ϵ-cages.

The onset of dynamic processes is different, when comparing the sodium cations interacting with chromate anions in the large channels (two sharp lines at 1.4 and −9.3 ppm) and without anion interaction in the small cages (broad quadrupolar component). While the two sharp signals begin to exhibit an exchange signal at 380 K, the motionally averaged signal for the quadrupolar line appears at a significantly higher temperature of 613 K. At the temperature of 498 K, where the broad quadrupolar component for sodium in the ϵ-cages can still clearly be identified, the sodium cations in the open channels with chromate anions have reached their full exchange dynamics already at 470 K. This clearly differs from the more dense sodalite structure. The dc conductivity of chromate cancrinite is very poor at 573 K. Its dc plateau is at 1.12×10^{-8} Ω^{-1} cm^{-1}. However, the activation energy of 89.2 kJ/mol is well in the expected range for anion-promoted local mobilities. This shows that local activation is not the problem for chromate cancrinite. The low dc conductivity is most likely due to the limitation in the dimensionality of cation transport. The sodium cations in the large channels can only move into one dimension, as, based on the ^{23}Na NMR data, no exchange with the smaller ϵ-cages takes place.

The ^{17}O MAS NMR spectrum of the chromate cancrinite also consists of a single narrow line, indicating a fast isotropic anion reorientation. In contrast to the sodalite, it was not possible to freeze out the anion motion even at the lowest accessible temperature of 130 K. Therefore, motional coupling between the anionic reorientation and the cation exchange process can be excluded because there is no correlation in their extent and onset of motion. A positive influence of fast anion reorientation on cation conductivity can be clearly ruled out for chromate cancrinite.

The lack of motional coupling between cations and anions is in line with an earlier study in our laboratory on tetrahydroxoborate sodalite with the unit cell composition $|Na_4B(OH)_4|_2[Al_6Si_6O_{24}]$−**SOD**. This sodalite shows a phase transition, accompanied by changes in the mobilities of the anions, $B(OH)_4^-$.[36] However, the NMR study also showed no symmetry equivalence of anion rotation and cation hopping. Local sodium motion was observed for this sodalite, and it was also interpreted as a two-site exchange, rather than an isotropic averaging by a full cation exchange between all sodium sites. It seems that such restricted sodium motions seem to be typical for sodalites.

The influence of the different anions on local cation motion and long-range transport has to be discussed under different aspects, as the applied methods yield information on different length and/or time scales. The theoretical modeling studies shown here and the NMR data focus on local properties, whereas the conductivity experiments are sensitive to larger length scales. It also should be noted that the simulations are single-point calculations on the energy landscape, where a dynamic time scale is not defined. Another difference between NMR and impedance spectroscopy is that the number densities of the moving ions may differ considerably. Good ion conductivity may arise from a defect mechanism, where a defect migrates very fast, but a vast majority of cations is rigid. For an NMR probe, this means that the materials appear to be static. It can only be expected that both methods give the same kind of information if the mobility of an appreciable number density of cations (rather than a small number of very mobile defects) contributes to charge transport. These properties should be kept in mind when comparing the different methods.

Simple isotropic anions, such as halides, promote the local cation site exchange by electrostatic interactions, decreasing the activation energy. On the other hand, steric influences of the larger halides increase again the activation barrier. For the larger complex chromate anions, local reorientations may also help to increase the cation site exchange, but we did not observe a coupling of cation and anion motions on the same time scale. A crucial factor for dc conductivities is the transport mechanism over a larger length scale. A cooperative motion of cations in different cages, such as in chromate sodalite, has a positive influence on three-dimensional cation transport. On the other hand, dc conductivities remain low despite high local mobilities when the cation motions in different cages/channels are not coupled, such as in chromate cancrinite. This scenario only allows for one-dimensional cation diffusion, which limits the dc conductivity.

The impact of anions on cation conduction will be part of our future studies. To achieve an appreciable long-range transport of cations, not only local mobilities are important, but also the existence of diffusional pathways is imperative.

Conclusions

The presence of anions promotes the local cation dynamics in zeolites. This conclusion is made from the theoretical force field calculations as well as from experimental evidence for sodalite and cancrinite with chromate anions. The force field calculations also show that the activation barrier for local cation diffusion is lower for the smaller anions, when comparing the

(36) Buhl, J. C.; Mundus, C.; Löns, J.; Hoffmann, W. *Z. Naturforsch.* **1994**, *49a*, 1171.

halogenide series, Cl^-, Br^-, and I^-. This trend is confirmed by dc conductivities and activation energies for these three sodalites with different halogenide fillings. In addition, the cation diffusion barrier of a pathway with higher oxygen coordination (four-ring route) is lower than that for low-coordinated pathways (oxygen bridge between two six-rings).

The local ion dynamics in chromate sodalite and chromate cancrinite show that the most favorable situation exists in the large channels of cancrinite, in which the chromate anions promote the cation exchange process. The cations in the smaller, anion-free ϵ-cages of cancrinite become mobile at much higher temperatures than the Na^+ cations which interact with the anions in the twelve-ring channels. The enhancement of local cation mobility by anion interaction is more efficient in the cancrinite structure, which has more space in the large channels (lower framework density).

There is no NMR evidence for a dynamics coupling between cationic and anionic motion in chromate sodalite and cancrinite. The chromate anions are highly mobile, and only in sodalite cages, they can be frozen out to an appreciable extent at 140 K. Chromate anions remain highly mobile at low temperatures in the large twelve-ring channels of cancrinite. Therefore, the onset of cation dynamics is not correlated with anion motion. The dc conductivity is highest for chromate sodalite, which also shows a cooperative onset of local cation motion. Therefore, cooperative effects of cations in different cages are important for three-dimensional cation conduction, which is higher than that in one-dimensional scenarios, as in chromate cancrinite. Lower framework densities of zeolites offer more space for local mobility enhancements by anion interactions, but motional couplings may be reduced by larger distances between the cations.

Future attempts to improve cation mobilities in zeolites with the aim to enhance ion conductivities should take into consideration the following recommendations: (1) local cation mobility can be improved by interaction with anions; (2) the promoting effect of anions on local motion is more efficient in a zeolite with lower framework densities; (3) diffusional pathways with high coordination in the transition state are favored over low coordination routes; and (4) cooperative cation diffusion mechanisms are important for dc conductivities.

Acknowledgment. Financial support by the Deutsche Forschungsgemeinschaft (SFB 458) is gratefully acknowledged.

JA0551887